Geometrical representation of coherent tunneling process in two-waveguide and three-waveguide coupler*

Jian Shi(时坚)†, Rui-Qiong Ma(马瑞琼), Zuo-Liang Duan(段作梁), Meng Liang(梁猛), Bao-Yu Chai(柴宝玉), and Jun Dong(董军)

School of Electronic Engineering, Xi'an University of Posts and Telecommunications, Xi'an 710121, *China*

(Received 9 May 2017; revised manuscript received 1 July 2017; published online 20 November 2017)

We propose an identical geometrical representation scheme for both Landau–Zener (LZ) tunneling process in two-waveguide coupler with a cubically bent structure and stimulated Raman adiabatic passage (STIRAP) in three-waveguide coupler, similar to the geometrical representation of sum frequency process. The results show that although the two-waveguide coupler with a cubically bent axis has not aperiodic structure, it acts as a chirped quasi-phase-matching (QPM) grating and corrects the relative phase between the two supermodes in the curved coupler system. We present a scheme about how to choose the parameters to design the curved beam splitter.

Keywords: optical coupler, adiabatic passage, non-adiabatic passage, Bloch vector

PACS: 42.82.Et, 42.65.Ky, 32.80.Qk **DOI:** 10.1088/1674-1056/26/12/124214

1. Introduction

Landau–Zener (LZ) non-adiabatic tunneling process and stimulated Raman adiabatic passage (STIRAP) have different physical mechanisms and have aroused wide interest during the past two decades. For instance, the former has been widely used in waveguide arrays,[1,2] electron transfer on insulating surface,[3] Bose–Einstein condensate,[4,5] Bose–Fermi mixture,[6] optical lattices,[7] radio frequency superconducting quantum interference,[8] preparation of quantum state,[9] coherent destruction of tunneling,[10] to name a few, while the latter has been used in waveguide optics,[11–13] population transfer in atomic and molecular physics,[14–18] Bose–Einstein condensate,[19,20] generation of terahertz pulses,[21] optical storage,[22] and so forth. Shore *et al.* have discussed the differences between the STIRAP in three-level atom system and LZ tunneling process in four-state model.[23]

Longhi proposed a simple two-waveguide device with cubically bent structure which can successfully mimic LZ tunneling process of a two-level atom system, and the results indicated that LZ tunneling efficiency is only about 55%.[24] Exploiting this dual-waveguide coupler, Dreisow *et al.* realized nearly 100% LZ tunneling efficiency and designed a beam splitter based on LZ dynamics in experiment,[25] but they did not indicate how to select the relevant parameters to design beam splitter. Using quasi-phase-matching (QPM) scheme,[26,27] Suchowski *et al.* successfully achieved nearly full conversion efficiency in sum frequency process under the undepleted pump condition, and they used Bloch vector to describe the process of optical sum frequency conversion intuitively.[28,29] In this paper, we discuss the similarities between coherent tunneling STIRAP-like equations of light in three-waveguide coupler, sum frequency adiabatic conversion equations, and LZ tunneling equations of light in curved two-waveguide coupler.

On one hand, by using the similarities between sum frequency equations and coupled equations of a three-waveguide coupler and the method proposed by Bloch[30] and Feynman *et al.*,[31] we construct Bloch geometric representation model of the three-waveguide system. From this geometrical viewpoint, we reanalyze the complicated behavior of light tunneling process in three-waveguide coupler. On the other hand, we analyze the similarity between sum frequency equations and LZ tunneling equations of a curved two-waveguide system, and this similarity allows a better understanding of the influences of spatial waveguide structure and phase mismatch. We find that this curved two-waveguide coupler can constantly adjust the phase difference between two supermodes in coupler system, like a chirped QPM grating, and finally it achieves arbitrary light intensity splitting ratio in left and right channels, providing that the appropriate spatial chirp coefficient is chosen. Furthermore, we give a parameter selection scheme about how to design a curved beam splitter. According to a more complex STIRAP three-waveguide system, we analyze another simpler two-waveguide system.

*Project supported by the National Natural Science Foundation of China (Grant Nos. 11304247 and 61505161) and the Shaanxi Provincial Research Plan for Young Scientific and Technological New Stars, China (Grant No. 2015KJXX-40).

†Corresponding author. E-mail: shijian@xupt.edu.cn

© 2017 Chinese Physical Society and IOP Publishing Ltd

2. Sum frequency coupled equations and three-waveguide coupled differential equations

2.1. Sum frequency coupled equations

Under the undepleted pump condition, the sum frequency coupled equations can be simplified into[29] $\mathrm{i}\mathrm{d}\tilde{A}_1/\mathrm{d}z = \kappa\tilde{A}_3\mathrm{e}^{-\mathrm{i}\Delta kz}$ and $\mathrm{i}\mathrm{d}\tilde{A}_3/\mathrm{d}z = \kappa\tilde{A}_1\mathrm{e}^{+\mathrm{i}\Delta kz}$, where κ is the coupling coefficient, Δk is the constant of phase mismatch, $\tilde{A}_1$ and $\tilde{A}_3$ are the complex amplitudes of signal and idler wave. Substituting $\tilde{A}_1(z) = A_1(z)\,\mathrm{e}^{-(\mathrm{i}\Delta k/2)z}$ and $\tilde{A}_3(z) = A_3(z)\,\mathrm{e}^{+(\mathrm{i}\Delta k/2)z}$ into the coupled equations, we can obtain

$$\mathrm{i}\frac{\mathrm{d}}{\mathrm{d}z}\begin{pmatrix} A_1(z) \\ A_3(z) \end{pmatrix} = \begin{pmatrix} -\dfrac{\Delta k}{2} & \kappa \\ \kappa & \dfrac{\Delta k}{2} \end{pmatrix}\begin{pmatrix} A_1(z) \\ A_3(z) \end{pmatrix}. \tag{1}$$

Equation (1) is similar to the coherent excitation equation of a two-level atom system in the rotating-wave approximation. Using Feynman *et al.*'s expression,[31] we can convert Eq. (1) into

$$\frac{\mathrm{d}}{\mathrm{d}z}\begin{pmatrix} U \\ V \\ W \end{pmatrix} = \begin{pmatrix} 0 & \Delta k & 0 \\ -\Delta k & 0 & 2\kappa \\ 0 & -2\kappa & 0 \end{pmatrix}\begin{pmatrix} U \\ V \\ W \end{pmatrix}, \tag{2}$$

where in Eq. (2), $U = A_1A_3^* + A_1^*A_3$, $V = \mathrm{i}(A_1A_3^* - A_1^*A_3)$, $W = A_3A_3^* - A_1A_1^*$, U, V, W are the three components of Bloch vector, which moves on a unit sphere surface if the two-state system is a pure state.

2.2. Three-waveguide coupled differential equations

In a three-waveguide coupler system shown in Fig. 1(a), the central waveguide is straight, the right and left waveguides are both parabolic. If incident light is coupled into the left channel, the right channel is coupled with the center channel before the left one, we call such a waveguide structure the counterintuitive tunneling scheme. The Ω_R and Ω_L in Fig. 1(b) are the tunneling rate distributions between two adjacent channels.

The coupled differential equations for a three-waveguide system take the following form:[13]

$$\mathrm{i}\frac{\mathrm{d}}{\mathrm{d}z}\begin{pmatrix} C_\mathrm{L}(z) \\ C_\mathrm{C}(z) \\ C_\mathrm{R}(z) \end{pmatrix} = \begin{pmatrix} 0 & -\Omega_\mathrm{L}(z) & 0 \\ -\Omega_\mathrm{L}(z) & 0 & -\Omega_\mathrm{R}(z) \\ 0 & -\Omega_\mathrm{R}(z) & 0 \end{pmatrix} \times \begin{pmatrix} C_\mathrm{L}(z) \\ C_\mathrm{C}(z) \\ C_\mathrm{R}(z) \end{pmatrix}, \tag{3}$$

where $C_\mathrm{L}(z)$, $C_\mathrm{C}(z)$, and $C_\mathrm{R}(z)$ are the complex amplitudes of light field in left ($|L\rangle$), central ($|C\rangle$) and right ($|R\rangle$) waveguides, $|C_\mathrm{n}(z)|^2$ indicates the variation of the light intensity along the propagation direction as seen in Eq. (3). The tunneling rate $\Omega_i(z)$ $(i = \mathrm{L},\mathrm{R})$ quantify the coherent tunneling passage between the adjacent waveguides. Equation (3) can be visualized on Bloch sphere, and if we redefine the following variables: $U = -C_\mathrm{R}(z)$, $V = -\mathrm{i}C_\mathrm{C}(z)$, $W = C_\mathrm{L}(z)$, the coupled differential equations Eq. (3) can be recast as

$$\frac{\mathrm{d}}{\mathrm{d}z}\begin{pmatrix} U \\ V \\ W \end{pmatrix} = \begin{pmatrix} 0 & \Omega_\mathrm{R}(z) & 0 \\ -\Omega_\mathrm{R}(z) & 0 & \Omega_\mathrm{L}(z) \\ 0 & -\Omega_\mathrm{L}(z) & 0 \end{pmatrix}\begin{pmatrix} U \\ V \\ W \end{pmatrix}. \tag{4}$$

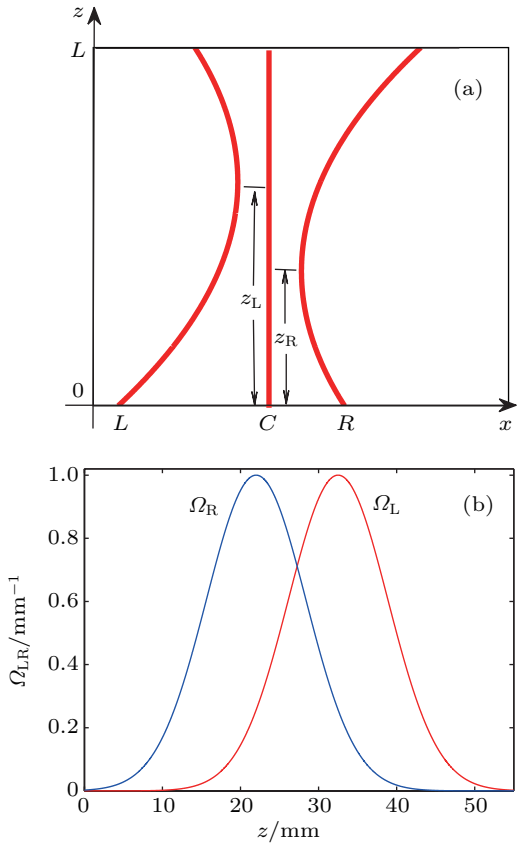


Fig. 1. (color online) Schematic diagrams of (a) three-waveguide coupler and (b) the distribution functions of the tunneling rate versus propagation distance.

Bloch vector $\boldsymbol{B}(z) = (U,V,W)^\mathrm{T}$ represents the energy relation in three-waveguide coupler. Equations (4) and (2) indicate that the coupled differential equations for a three-waveguide system are completely equivalent to sum frequency Bloch equations, the phase mismatch Δk and the two times of coupling coefficient 2κ are replaced by tunneling rate $\Omega_\mathrm{R}(z)$ and $\Omega_\mathrm{L}(z)$, respectively, the superposition of idler (A_3) and signal(A_1) fields are replaced by the complex amplitude of light field in waveguide, the final tunneling efficiency η between left and right channels can be set up by x and z components of Bloch vector $\boldsymbol{B}(z)$,

$$\eta(+\infty) = \frac{1 + |C_\mathrm{R}(+\infty)|^2 - |C_\mathrm{L}(+\infty)|^2}{2} = \frac{1 + |U|^2 - |W|^2}{2},$$

the north pole vector $\boldsymbol{B}(z) = (0,0,1)^\mathrm{T}$ means zero conversion ($C_\mathrm{R} = 0$), while the equatorial vector $\boldsymbol{B}(z) = (1,0,0)^\mathrm{T}$ corresponds to the full tunneling conversion ($C_\mathrm{R} = 1$). The mechanism of the coherent tunneling process in three-waveguide directional coupler can be easily understood if we derive the

instantaneous eigenvectors $|\Phi_+(z)\rangle$, $|\Phi_0(z)\rangle$, $|\Phi_-(z)\rangle$ of the tunneling rate matrix of Eq. (3):

$$|\Phi_+(z)\rangle = \frac{1}{\sqrt{2}}(\sin\theta\,|L\rangle + |C\rangle + \cos\theta\,|R\rangle), \tag{5a}$$

$$|\Phi_0(z)\rangle = \cos\theta\,|\mathrm{L}\rangle - \sin\theta\,|R\rangle\,, \tag{5b}$$

$$|\Phi_-(z)\rangle = \frac{1}{\sqrt{2}}(\sin\theta\,|L\rangle - |C\rangle + \cos\theta\,|R\rangle). \tag{5c}$$

Defining the space-dependent mixing angle $\theta(z)$ as

$$\tan\theta(z) = \frac{\Omega_{\mathrm{L}}(z)}{\Omega_{\mathrm{R}}(z)}, \tag{6}$$

and introducing new variable $\tilde{\Omega}_0(z) = \sqrt{\Omega_{\mathrm{L}}^2(z) + \Omega_{\mathrm{R}}^2(z)}$, we can obtain the adiabatic condition

$$\left|\frac{\dot{\theta}(z)}{\tilde{\Omega}_0(z)}\right| = \left|\frac{\dot{\Omega}_{\mathrm{L}}(z)\Omega_{\mathrm{R}}(z) - \dot{\Omega}_{\mathrm{R}}(z)\Omega_{\mathrm{L}}(z)}{\left(\Omega_{\mathrm{L}}^2 + \Omega_{\mathrm{R}}^2\right)^{3/2}}\right| \ll 1. \tag{7}$$

The dot represents the derivative with respect to$z$. During the STIRAP in three-waveguide system, the initial adiabatic state points along the state $|\Phi_0(-\infty)\rangle = |L\rangle$, in order to maintain a continuous alignment of this adiabatic state with the trapped state $|\Phi_0(z)\rangle$, the adiabatic tunneling condition shall be fulfilled, and the tunneling rate Ω_{R} between the right and central waveguides must precede Ω_{L} which is the tunneling rate between the left and central ones. Choosing proper tunneling rate distribution functions can adjust the mixing angle $\theta(z)$, and further control the proportion of light intensity in left and right waveguides.

3. Geometrical representation of STIRAP in three-waveguide coupler

In the counterintuitive three-waveguide tunneling scheme, Ω_{R} precedes Ω_{L}. The initial mixing angle $\theta(-\infty) \approx 0$, the initial dark state $\Phi_0(-\infty) = |L\rangle$, then, as the propagation distance z approaches to infinity, $\theta(+\infty) \approx \pi/2$, the final dark state $\Phi_0(+\infty) = |R\rangle$. Figure 2 shows the movement tracks of Bloch vector for three kinds of adiabatic tunneling processes in counterintuitive coupled system with different tunneling rate distributions and one non-adiabatic passage in intuitive system.

In full efficiency STIRAP scheme, figure 2(a) shows that Bloch vector which is composed of U, V, and W moves on the Bloch unit sphere from the north pole to the equator slightly deviated from longitude. From the dark state expression $|\Phi_0(z)\rangle = \cos\theta\,|L\rangle - \sin\theta\,|R\rangle$, the initial mixing angle $\theta(-\infty) = 0$, the initial z component $W(-\infty) = 1$, $I_{\mathrm{L}} = C_{\mathrm{L}}(-\infty)C_{\mathrm{L}}^*(-\infty) = WW^* = |W|^2 = 1$, in the output plane, $\theta(+\infty) = \pi/2$, $W(+\infty) = 0$, $U(+\infty) = 1$, $I_{\mathrm{R}} = C_{\mathrm{R}}(+\infty)C_{\mathrm{R}}^*(+\infty) = UU^* = |U|^2 = 1$, light power transfers to the right waveguide, and these finial states correspond to maximum coherence states in a two-state atom system. During adiabatic tunneling evolution, it is not easy to calculate the tunneling efficiency η at any position along the propagation direction, because V component of Bloch vector is not zero, but at the output end of the system, the tunneling efficiency can be easily seen from the Bloch sphere $\eta(+\infty) = |U(+\infty)|^2 = 1$.

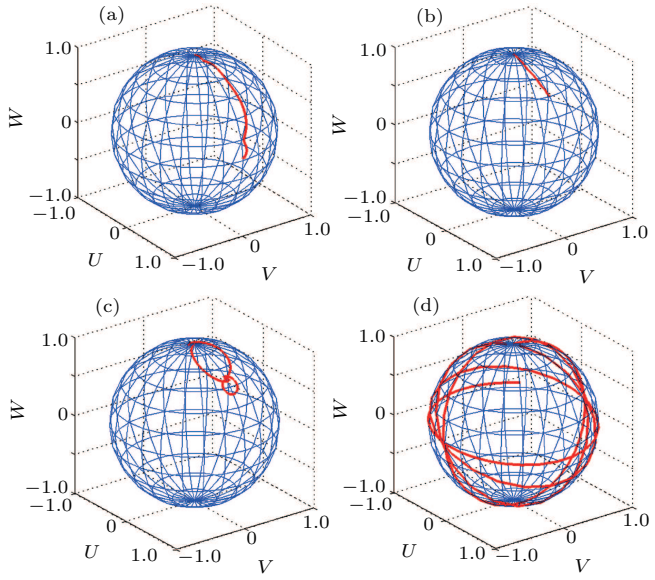


Fig. 2. (color online) Geometrical visualizations of STIRAP in three-waveguide directional couplers: (a) full efficiency STIRAP, (b) fractional efficiency STIRAP, (c) zero efficiency STIRAP, and (d) non-adiabatic passage. In all of these schemes, the light is coupled into the left waveguide, and the selected adiabatic tunneling rate parameters are the same as those in Ref. [13]. While in non-adiabatic scheme, the parameters are $z_{\mathrm{R}} = 30.5$ mm, $z_{\mathrm{L}} = 22$ mm, $\zeta_{\mathrm{R}} = \zeta_{\mathrm{L}} = 9$ mm, $\Omega = 1$ mm^{-1}, $\Omega_{\mathrm{R}}(z) = \Omega\exp[-(z-z_{\mathrm{R}})^2/\zeta_{\mathrm{R}}^2], \Omega_{\mathrm{L}}(z) = \Omega\exp[-(z-z_{\mathrm{L}})^2/\zeta_{\mathrm{L}}^2]$.

In fractional efficiency STIRAP scheme, Ω_{R} still precedes Ω_{L}. Unlike the STIRAP, with the propagation distance tending to infinity, $\Omega_{\mathrm{R}} = \Omega_{\mathrm{L}}$, these two tunneling rate distributions vanish together in the same proportion, and the Bloch vector $\boldsymbol{B}(z)$ rotates around one longitude in the WU plane as shown in Fig. 2(b). The initial mixing angle, $I = C_{\mathrm{L}}(-\infty)C_{\mathrm{L}}^*(-\infty) = WW^* = |W|^2 = 1$, on the output plane, $\theta(+\infty) = \pi/4$, $W(+\infty) = \cos\theta(+\infty) \approx 0.7$, $U(+\infty) = \sin\theta(+\infty) \approx 0.7$, $V(+\infty) = 0$, $I_{\mathrm{L}} = C_{\mathrm{L}}(+\infty)C_{\mathrm{L}}^*(+\infty) = WW^* = |W|^2 \approx 0.5$, $I_{\mathrm{R}} = C_{\mathrm{R}}(+\infty)C_{\mathrm{R}}^*(+\infty) = UU^* = |U|^2 \approx 0.5$, light power is divided equally between the right and left waveguides. During this adiabatic evolution, $V(z)$ is so small that the light power in central waveguide almost approaches to zero $I_{\mathrm{C}} = C_{\mathrm{C}}(z)C_{\mathrm{C}}^*(z) = VV^* = |V|^2 \approx 0$. Throughout the fractional STIRAP, we can visually see the tunneling efficiency η from the U component of Bloch vector $\boldsymbol{B}(z)$ because $\eta(z) = (1 + |U(z)|^2 - |W(z)|^2)/2 = |U(z)|^2$.

In a zero efficiency STIRAP scheme, Ω_{R} precedes Ω_{L} at very early distance, but vanishes more slowly than Ω_{L} at very later distance, Bloch vector $\boldsymbol{B}(z)$ deviates from the longitude which is parallel to the WU plane, and finally it goes back to the starting point as shown in Fig. 2(c). Al-

though this process is also adiabatic evolution, the value of the deviation $V(z)$ is large, $V(z)_{\max} = 0.2$, the maximum light power in central waveguide $I_{\mathrm{Cmax}} = C_{\mathrm{Cmax}} C^*_{\mathrm{Cmax}} = |V|^2_{\max} = 0.04$, which indicates that the energy in central waveguide is nearly zero. At the output of the coupler, $\theta(+\infty) = 0$, $W = 1$, $U = 0$, $I_{\mathrm{L}} = C_{\mathrm{L}}(+\infty) C^*_{\mathrm{L}}(+\infty) = WW^* = |W|^2 = 1$, $I_{\mathrm{R}} = C_{\mathrm{R}}(+\infty) C^*_{\mathrm{R}}(+\infty) = UU^* = |U|^2 = 0$, light power transfers back to the left waveguide again. The deviation value $V(z)$ is bigger, so we cannot directly see the conversion efficiency of the entire adiabatic process from Bloch vector, except at the terminal point of the tunneling passage.

In the non-adiabatic scheme, the tunneling rate Ω_{L} precedes Ω_{R}, $\theta(-\infty) \approx \pi/2$, the initial state vector is composed of two instantaneous eigenvectors $|\Phi_+(z)\rangle$ and $|\Phi_-(z)\rangle$, i.e., $|\Phi(-\infty)\rangle = [|\Phi_+(-\infty)\rangle + |\Phi_-(-\infty)\rangle]/\sqrt{2} = |L\rangle$, thereby it does not align with the trapped state $|\Phi_0(-\infty)\rangle = |L\rangle$ any more as seen in Eqs. (5a) and (5c). Since this is a non-adiabatic evolution process, coherent superposition occurs between the adiabatic states with the increasing of the propagation distance, and the light energy tunnels between the two adjacent waveguides and transfers as Rabi-like oscillations. Bloch vector $\boldsymbol{B}(z)$, which experiences several big circles, rotates on Bloch sphere from the north pole to the equator as shown in Fig. 2(d). This trajectory describes the multiple exchange of light power among all three channels. Later, when the propagation distance approaches to infinity, i.e., $z \to +\infty$, then $I_{\mathrm{L}}(+\infty) = 0$, $I_{\mathrm{C}}(+\infty) = \sin^2\zeta$, and $I_{\mathrm{R}}(+\infty) = \cos^2\zeta$, where $\zeta = \int_{-\infty}^{+\infty} \tilde{\Omega}_0(z)\mathrm{d}z$.

With angular velocity vector defined as $\boldsymbol{\Omega}(z) = [-\Omega_{\mathrm{L}}(z), 0, -\Omega_{\mathrm{R}}(z)]^{\mathrm{T}}$, using the symmetrical characteristic of Eq. (4), we can convert Eq. (4) into a torque equation:

$$\frac{\mathrm{d}}{\mathrm{d}z}\boldsymbol{B}(z) = \boldsymbol{\Omega}(z) \times \boldsymbol{B}(z). \tag{8}$$

As in classical dynamics, a force $\boldsymbol{\Omega}(z) \times \boldsymbol{B}(z)$ which is perpendicular to Bloch vector $\boldsymbol{B}(z)$ can change the movement of Bloch vector. Taking into account both the definition of the space-dependent mixing angle $\theta(z)$ and assumptions $U = -C_{\mathrm{R}}(z)$, $W = C_{\mathrm{L}}(z)$, the dark state Eq. (5b) can be rewritten in terms of the components of the angular velocity vector $\boldsymbol{\Omega}(z)$ and Bloch vector $\boldsymbol{B}(z)$ as follows:

$$\Omega_0(z) = \frac{U\Omega_{\mathrm{L}}(z) + W\Omega_{\mathrm{R}}(z)}{\tilde{\Omega}_0(z)}, \tag{9}$$

where we have set $\tilde{\Omega}_0(z) = \sqrt{\Omega^2_{\mathrm{L}}(z) + \Omega^2_{\mathrm{R}}(z)}$, according to the torque equation (8), the ideal STIRAP in three-waveguide coupler can be understand from this new standpoint as shown in Fig. 3. Initially the angular velocity vector $\boldsymbol{\Omega}(z)$ and Bloch vector $\boldsymbol{B}(z)$ are both parallel to the W axis (z axis), so Bloch vector $\boldsymbol{B}(z)$ stays still. With the introduction of the counterintuitive tunneling rate distribution, the angular velocity vector $\boldsymbol{\Omega}(z)$ begins to rotate, and the rotation direction of the angular velocity vector depends on counterintuitive tunneling scheme. Since this is adiabatic evolution process, Bloch vector $\boldsymbol{B}(z)$ follows the angular velocity vector $\boldsymbol{\Omega}(z)$. Finally, the angular velocity vector $\boldsymbol{\Omega}(z)$ and Bloch vector $\boldsymbol{B}(z)$ are still parallel to each other along a certain direction in the WU plane.

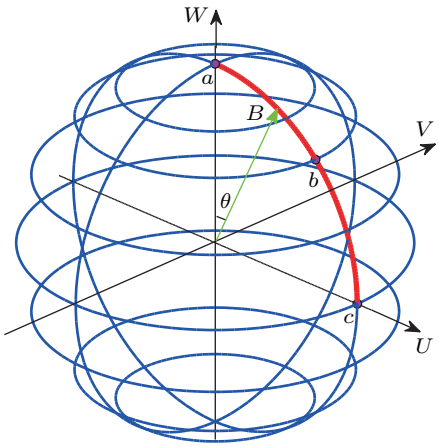


Fig. 3. (color online) Geometrical representation of ideal STIRAP in three-waveguide directional coupler, the central waveguide is not excited.

According to the resemblance between the three-waveguide coupled differential equations and the sum frequency coupled equations under the undepleted pump condition, we construct the three real-valued Bloch variables by using the three components of the light field complex amplitude. Expressions (5b) and (7) show that in order to achieve the STIRAP in three-waveguide coupler, we should select suitable tunneling rate distributions Ω_{L} and Ω_{R} to control Bloch vector moving along the arc $\overset{\frown}{abc}$ and simultaneously minimize V component as sketched in Fig. 3. For this reason, we must consider two aspects to choose Ω_{L} and Ω_{R}. On the one hand, the parameter θ which is defined by Eq. (6) can describe the angle between Bloch vector $\boldsymbol{B}$ and one component W, and by selecting the proper tunneling rate parameters we can control this angle distribution function, $|W|^2 = \cos^2(\theta)$ and $|U|^2 = \sin^2(\theta)$, which can indicate the light powers in the left and right channels, respectively, on the other hand, the component V, namely the deviation between Bloch trajectory and the arc $\overset{\frown}{abc}$, can indirectly represent whether the adiabatic condition is met as can be seen from both Fig. 2 and Fig. 4. A smaller absolute value of V indicates that the adiabatic condition is satisfied, and a bigger absolute value of V indicates that the adiabatic condition is destroyed. In full efficiency STIRAP scheme, we want to control Bloch vector to move from point a to point c. Figures 2(a) and 4 indicate that the biggest component V corresponds to $\left|\dot{\theta}/\tilde{\Omega}_0\right| \approx 0.13$ and the adiabatic condition is no longer much less than one, so the light power tunnels into the middle waveguide. By choosing the best distance between the peck values of the

tunneling rate $\Omega_{\rm L}$ and $\Omega_{\rm R}$, we can reduce the value V, and the distance used here is already the best choice. In fractional efficiency STIRAP scheme, using the tunneling rate distributions $\Omega_{\rm L}(z) = \Omega \sin\theta_0 \exp[-(z-z_{\rm L})^2/\zeta_{\rm L}^2]$ and $\Omega_{\rm R}(z) = \Omega \exp[-(z-z_{\rm R})^2/\zeta_{\rm R}^2] + \Omega \cos\theta_0 \exp[-(z-z_{\rm L})^2/\zeta_{\rm L}^2]$, we can control Bloch vector to move from point a to an arbitrary point on the arc $\overset{\frown}{abc}$. The parameters are defined in Ref. [13]. In these two expressions, the parameter θ_0 corresponds to the angle θ between Bloch vector $\boldsymbol{B}$ and the component W. During STIRAP, the adiabatic condition is always satisfied as shown in Fig. 4. If we control the parameter θ_0, we can achieve an arbitrary light intensity splitting ratio in left and right channels. When $\theta_0 = \pi/4$, the light energy is split equally into left and right waveguides. Figure 4 shows that there are two diabatic points in zero efficiency STIRAP, this leads to big discrepancy between Bloch trajectory and the arc $\overset{\frown}{abc}$, namely big V value, as indicated in Fig. 2(c). We can choose the better tunneling rate distributions to achieve STIRAP, for example, $\Omega_{\rm L}(z) = \Omega \exp[-(z-z_{\rm L})^2/\zeta_{\rm L}^2]$, $\Omega_{\rm R}(z) = \Omega \exp[-(z-z_{\rm R})^2/\zeta_{\rm R}^2]$, $z_{\rm R} = z_{\rm L} = 30$ mm, $\zeta_{\rm R} = 80$ mm, $\zeta_{\rm L} = 10$ mm, $\Omega = 1$ mm^{-1}. Under such conditions, Bloch vector gets back to the starting point, the big discrepancy can be reduced, which means that the light power tunnels little into the middle waveguide.

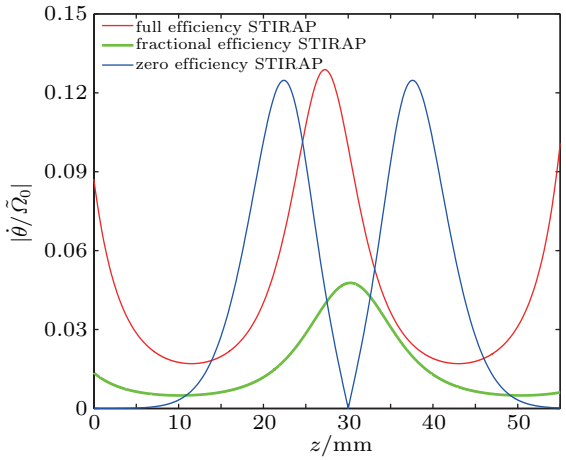


Fig. 4. (color online) Adiabatic condition evolutions along the three-waveguide coupler in different stimulated Raman adiabatic schemes.

4. Geometrical representation of LZ tunneling process in bent two-waveguide coupler

Longhi[24] proposed a cubically bent two-waveguide device to mimic LZ tunneling process of a two-level atom system as shown in Fig. 5. The length of the optical coupler system is L, two adjacent identical channels are separated by a distance a, and the transverse maximum distance between input and output port is $2A$. The following two-waveguide coupled differential equations are derived:

$$\frac{{\rm d}\tilde{A}_1}{{\rm d}z} = -{\rm i}\kappa z\tilde{A}_1 - {\rm i}\frac{\Delta\beta}{2}\tilde{A}_2, \tag{10a}$$

$$\frac{{\rm d}\tilde{A}_2}{{\rm d}z} = {\rm i}\kappa z\tilde{A}_2 - {\rm i}\frac{\Delta\beta}{2}\tilde{A}_1, \tag{10b}$$

where $\Delta\beta = \beta_1 - \beta_2$ is the shift of propagation constant, β_1 and β_2 are the eigenvalues of stationary supermodes wave functions, and $\tilde{A}_1$ and $\tilde{A}_2$ are the complex amplitudes of the supermode superposition of the coupled waveguides, which can refer to the amplitudes of the light in the left and right waveguides. So $|\tilde{A}_1|^2$ and $|\tilde{A}_2|^2$ can describe the beam power evolutions along the$z$direction in two channels. Multiply both sides of Eqs. (10a) and (10b) with $\exp({\rm i}\kappa z^2/2)$ and $\exp(-{\rm i}\kappa z^2/2)$, respectively, then we will obtain

$$\frac{\rm d}{{\rm d}z}\left(\tilde{A}_1 \exp\left({\rm i}\frac{\kappa}{2}z^2\right)\right) = -{\rm i}\frac{\Delta\beta}{2}\tilde{A}_2 \exp\left({\rm i}\frac{\kappa}{2}z^2\right),$$
$$\frac{\rm d}{{\rm d}z}\left(\tilde{A}_2 \exp\left(-{\rm i}\frac{\kappa}{2}z^2\right)\right) = -{\rm i}\frac{\Delta\beta}{2}\tilde{A}_1 \exp\left(-{\rm i}\frac{\kappa}{2}z^2\right).$$

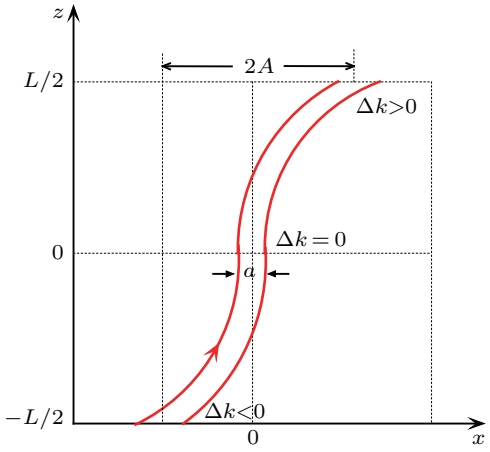


Fig. 5. (color online) Schematic diagram of a two-waveguide coupler with cubically bent structure.

If we make the following substitutions: $\tilde{A}_1 \exp({\rm i}\frac{\kappa}{2}z^2) = A_1$, $\tilde{A}_2 \exp(-{\rm i}\frac{\kappa}{2}z^2) = A_2$, $\Delta k = \kappa z$, these two equations can be converted into

$$\frac{{\rm d}A_1}{{\rm d}z} = -{\rm i}\frac{\Delta\beta}{2}A_2 {\rm e}^{{\rm i}\Delta k z}, \tag{11a}$$

$$\frac{{\rm d}A_2}{{\rm d}z} = -{\rm i}\frac{\Delta\beta}{2}A_1 {\rm e}^{-{\rm i}\Delta k z}. \tag{11b}$$

As indicated by Longhi, the coupling constant $\kappa = 48\pi a A {\rm n_s}/(\lambda L^3)$, where λ is the optical wavelength in channel and $\rm n_s$ is the substrate refractive index. It is easy to see that κ is a positive constant proportional to A when other physical quantities are all fixed constants. However, as we borrow the chirped quasi-phase-matching (QPM) grating theory and further analyze the analogy between Eqs. (11a), (11b), and sum frequency coupled equations, we can consider the coupling constant κ as the grating chirp coefficient.

There are two supermodes in the two-waveguide system, one is even supermode with the propagation constant β_1 and the other is odd supermode with the propagation constant β_2, and $\beta_1 > \beta_2$. When two channels are straight, at the input of the coupler $z = 0$ the initial phase difference $\Delta\Phi = \Phi_{\rm R} - \Phi_{\rm L} =$

0, so we have a constructive superposition in left waveguide and a destructive superposition in right waveguide. The beam power is confined in the left channel, because the two modes have different speeds. The phase difference $\Delta\Phi$ between the right waveguide $\Phi_{\rm R}$ and the left waveguide $\Phi_{\rm L}$ varies with the propagation distance z, especially, at a certain distance, the phase difference $\Delta\Phi = \Phi_{\rm R} - \Phi_{\rm L} = \pi$, which means that we have a constructive superposition in the right waveguide and a destructive superposition in the left waveguide, the beam power tunnels into the right channel. The values of $\Delta\Phi$ can take 2π, 3π, 4π, 5π, ... with the spreading distance increasing. When $\Delta\Phi$ takes an even number of π, the beam power stays in the left channel, when $\Delta\Phi$ takes an odd number of π, the beam power stays in the right channel. The beam power hops between the left and right waveguides, like Rabi oscillation in a two-level atomic system. But when the two waveguides have a cubically bent structure, in three different cases: $z < 0$, $z = 0$, $z > 0$, the values of the new variable $\Delta k = \kappa z$ are negative, zero and positive, respectively. Different value distributions of Δk have a striking similarity to a chirped QPM grating. Although this particular structure has not an aperiodic structure, it can correct the relative phase between the two supermodes as a chirped QPM grating. Changing the parameters A, a and L, we can achieve 100% LZ tunneling efficiency or achieve an arbitrary light intensity splitting ratio in the left and right channels.

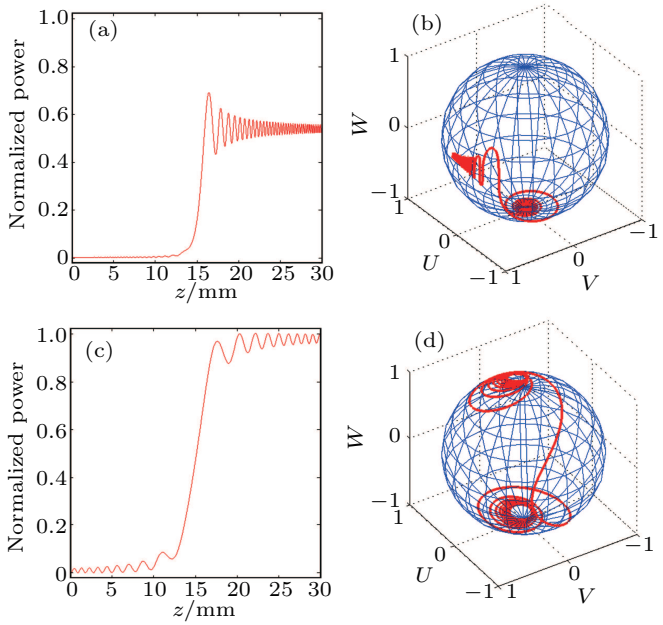


Fig. 6. (color online) Beam intensity evolution in the left channel versus propagation distance$z$ and its corresponding Bloch vector trajectory. The parameters are [(a) and (b)] $A = 16$ mm, $\kappa = 1$ mm^{-2}, and [(c) and (d)] $A = 4$ mm, $\kappa = 0.25$ mm^{-2}.

We choose $\Delta\beta = 1.013$ mm^{-1}, $n_s = 2.138$, $\lambda = 1.55$ μm, $a = 8$ μm, and $L = 30$ mm to stimulate Eqs. (11a) and (11b). In a two-waveguide optical coupler with a cubically bent structure, Landau–Zener dynamic tunneling efficiency is about 55%. The geometrical representation of LZ coupled equations (11a) and (11b) are shown in Fig. 6(b). Note that in an adiabatic sum frequency conversion process, the up-conversion efficiency can reach 99% due to the existence of the suitable phase mismatch value Δk. In order to improve the LZ tunneling efficiency of the two-waveguide optical coupler system, we can reduce the grating chirp coefficient κ. Surely full energy transfer can be achieved in the cubic bent two-waveguide coupler as shown in Figs. 6(c) and 6(d).

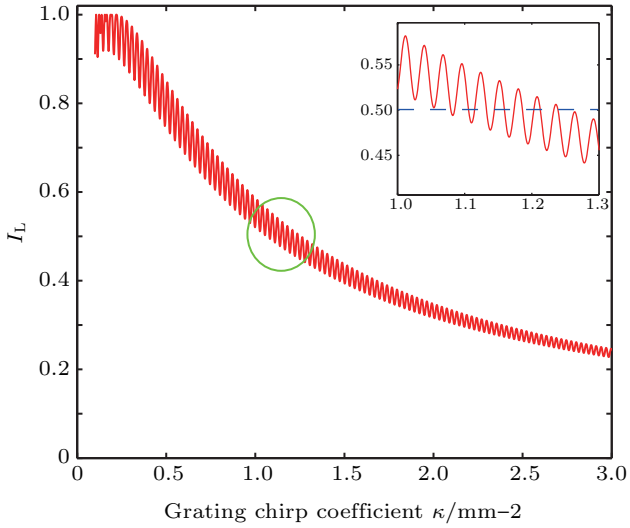


Fig. 7. (color online) Normalized light intensity at the output port of left channel versus grating chirp coefficient.

As shown in Figs. 6(a) and 6(c), the value of beam intensity near the coupler output port possesses an oscillation characteristic, so the normalized light intensity at the output port of the left channel is not monotonically decreasing function with the increasing of grating chirp coefficient κ, it has also an oscillation characteristic as indicated in Fig. 7. In order to design a beam splitter we can use the results of Fig. 7. Enlarging the circular region in Fig. 7, we find that there are thirteen points of intersection between horizontal dash line (LZ tunneling efficiency is 50%) and the curve of the normalized beam intensity at the output port of the left channel, and each horizontal coordinate of the intersection point can be used to design a beam splitter. When designing the desired beam splitters in various sizes, we must first consider the distance between the two adjacent waveguides a, because if a gets bigger, the tunneling rate between channels gets smaller. When $a = 13$ μm, the tunneling rate comes down almost to zero,[12] and we cannot infinitely increase a. Substituting these horizontal coordinates of intersection point κ into the grating chirp coefficient expression $\kappa = 48\pi a A n_s/(\lambda L^3)$, for fixed distance between the two adjacent waveguides a and longitudinal length of the coupler L, we can design a series of beam splitters with different values of transverse size $2A$, and for fixed a and A, we can design a series of beam splitters with different values of longitudinal size L. It can be seen from the grating chirp coefficient expression that A is proportional to the cubed L, with grating chirp coefficient κ and a fixed. Therefore the length of the beam splitter

has a greater influence on transverse size of beam splitter than other physical quantities.

5. Further discussion about dual-waveguide coupler based on three-waveguide coupler

When the two waveguides are both straight, $A=0$, $\kappa=0$, the light intensity evolution along two-waveguide coupler is similar to Rabi oscillation in a two-level atomic system. To avoid this situation, we calculate the light intensity at the output port of left channel under the condition $\kappa \geq 0.1$ as shown in Fig. 7.

In the three-waveguide coupler system as shown in Fig. 1(a), the tunneling rate distributions $\Omega_{\mathrm{R}}(z)$ and $\Omega_{\mathrm{L}}(z)$ of the right and left channels from the central one are both Gaussian profiles, so this system can easily achieve STIRAP. If the left waveguide is removed, the rest of this system is a two-waveguide coupler as shown in Fig. 8. For such a two-waveguide coupler, three-waveguide coupled equations (Eq. (3)) are reduced to two-waveguide coupled equations

$$\mathrm{i}\frac{\mathrm{d}}{\mathrm{d}z}C_{\mathrm{L}}(z) = -\Omega(z)C_{\mathrm{R}}(z), \tag{12a}$$

$$\mathrm{i}\frac{\mathrm{d}}{\mathrm{d}z}C_{\mathrm{R}}(z) = -\Omega(z)C_{\mathrm{L}}(z), \tag{12b}$$

which are different from Eqs. (10a) and (10b) due to the difference in dual-waveguide coupler structure. In Eqs. (12a) and (12b), C_{L} and C_{R} are the complex amplitudes of light field in the left and right channels respectively. The expression $\Omega(z)=\Omega_0\exp[-(z-z_0)^2/\zeta^2]$ is the tunneling rate between two adjacent waveguides. Equations (12a) and (12b) are similar to the two-state resonant excitation equations in the rotating wave approximation (RWA). Adjusting the distribution of the tunneling rate function and the peak tunneling rate value Ω_0, we can produce any desired energy distribution, from no energy transfer to full energy transfer. Selecting the following parameters: $\Omega_0=1.4\ \mathrm{mm}^{-1}$, $z_0=20$ mm, and $\zeta=9.5$ mm, we can obtain another beam splitter based on resonant excitation theory which is different from that based on LZ tunneling mechanism.

We can see that LZ coupled equations (10) have similarities to the sum frequency coupled equations (1). so it is easy for us to write out the following expression of Bloch vector for a curved two-waveguide system similar to Eq. (2).

$$\frac{\mathrm{d}}{\mathrm{d}z}\begin{pmatrix}U\\V\\W\end{pmatrix} = \begin{pmatrix}0 & -2\kappa z & 0\\ 2\kappa z & 0 & \Delta\beta\\ 0 & -\Delta\beta & 0\end{pmatrix}\begin{pmatrix}U\\V\\W\end{pmatrix}. \tag{13}$$

Using the similarities between Eqs. (13) and (4) and introducing new variables: $\tan\theta(z)=\Delta\beta/-2\kappa z$ and $\tilde{\Omega}_0(z)=\sqrt{\Delta\beta^2+(2\kappa z)^2}$, we obtain the corresponding adiabatic criterion Eq. (14) without solving the eigenvalues and seeking the expressions for the eigenvector components of Eq. (10) in dressed states picture.

$$\left|\frac{\dot{\theta}(z)}{\tilde{\Omega}_0(z)}\right| = \left|\frac{2\kappa\Delta\beta}{(\Delta\beta^2+(2\kappa z)^2)^{3/2}}\right| \ll 1. \tag{14}$$

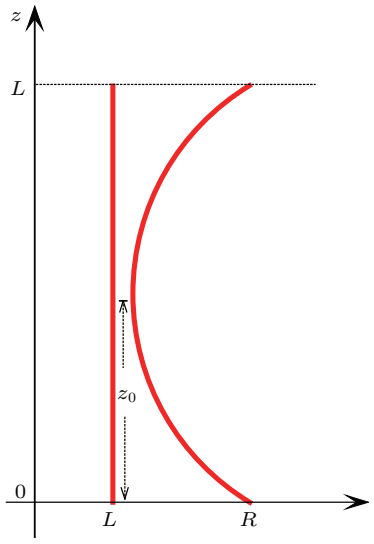


Fig. 8. (color online) Schematic diagram of two-waveguide coupler.

In the intermediate section of the curved dual-waveguide system, the condition $\left|\dot{\theta}(z)/\tilde{\Omega}_0(z)\right| \ll 1$ fails to hold, the LZ tunneling process occurs when the light passes through this region as indicated in Fig. 9 and Figs. 6(a) and 6(c). When the value $\left|\dot{\theta}(z)/\tilde{\Omega}_0(z)\right|$ gets bigger, adiabatic condition acts as a long straight edge, and the LZ tunneling process in two-waveguide coupler system is analogous to the Fresnel straight edge diffraction in traditional optics.

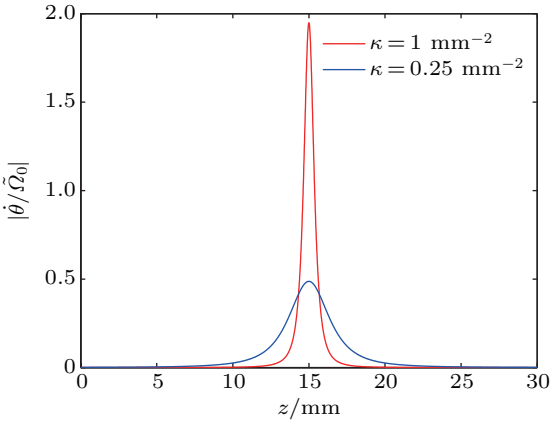


Fig. 9. (color online) Adiabatic condition evolution along the curved two-waveguide coupler in LZ tunneling scheme.

6. Conclusions

In this paper, first, we use the analogy between the equations of chirped sum frequency conversion and three-waveguide STIRAP to construct Bloch vector of three-state system, and under adiabatic or non-adiabatic condition, we describe the tunneling process of optical energy in the three-waveguide directional coupler by using Bloch vector. Then, after simple mathematical transformation, we find that the sum

frequency process using a chirped QPM grating and LZ tunneling process in dual-waveguide with a bent axis bear an intriguing similarity. This particular cubically curved two-waveguide coupler can provide suitable chirp factor similar to a chirped QPM grating. By choosing the appropriate spatial chirp coefficient to correct the relative phase between two supermodes, we can control the distribution of light intensity in this curved two-waveguide system. For fixed wavelength λ, there exist different sets of parameters to design beam splitters with various sizes, and the parameters can be chosen very flexibly. Finally, based on three-waveguide coupler, we analyze another two-waveguide coupler which is based on resonant coherent tunneling principle.

During the past decade, STIRAP in multi-waveguide coupled systems has been studied in detail, so it is possible for us to learn something about a simpler curved two-waveguide coupler from a more complex three-waveguide system. In analogy with the three-waveguide Bloch equations, we can easily obtain the adiabatic condition of the curved two-waveguide without complex calculation steps, and this condition can help us to analyze the LZ tunneling process in a curved two-waveguide system.

References

[1] Khomeriki R and Ruffo S 2005 *Phys. Rev. Lett.* **94** 113904
[2] Fratalocchi A and Assanto G 2006 *Opt. Express* **14** 2021
[3] Zhou W, Zhang M X, Zhou L H, Zhou H, Ma Y L, Guo Y L, Chen L and Chen X M 2016 *Chin. Phys. B* **25** 113401
[4] Olson A J, Wang S J, Niffenegger R J, Li C H, Greene C H and Chen Y P 2014 *Phys. Rev. A* **90** 013616
[5] Gomez Llorente J M and Plata J 2016 *Phys. Rev. A* **94** 053605
[6] Zhang H, Wang W Y, Meng H J, Ma Y, Ma Y Y and Duan W S 2013 *Acta Phys. Sin.* **62** 110305 (in Chinese)
[7] Salger T, Geckeler C, Kling S and Weitz M 2007 *Phys. Rev. Lett.* **99** 190405
[8] Shi J X, Xu W W, Sun G Z, Chen J, Kang L and Wu P H 2017 *Chin. Phys. B* **26** 047402
[9] Saito K, Wubs M, Kohler S, Hanggi P and Kayanuma Y 2006 *Europhys. Lett.* **76** 22
[10] Kayanuma Y and Saito K 2008 *Phys. Rev. A* **77** 010101
[11] Shi J, Ma R Q, Duan Z L, Liang M, Zhang W W and Dong J 2016 *Opt. Commun.* **370** 29
[12] Longhi S, Valle G D, Ornigotti M and Laporta P 2007 *Phys. Rev. B* **76** 201101
[13] Paspalakis E 2006 *Opt. Commun.* **258** 30
[14] Vitanov N V and Shore B W 2006 *Phys. Rev. A* **73** 053402
[15] Shore B W, Rangelov A A and Vitanov N V 2010 *Opt. Commun.* **283** 730
[16] Du Y X, Liang Z T, Huang W, Yan H and Zhu S L 2014 *Phys. Rev. A* **90** 023821
[17] Li J, Liu Y and Cong S L 2014 *Chin. Phys. B* **23** 010308
[18] Vitanov N V, Rangelov A A, Shore B W and Bergmann K 2017 *Rev. Mod. Phys.* **89** 015006
[19] Drummond P D, Kheruntsyan K V, Heinzen D J and Wynar R H 2002 *Phys. Rev. A* **65** 063619
[20] Dupont-Nivet M, Casiulis M, Laudat T, Westbrook C I and Schwartz S 2015 *Phys. Rev. A* **91** 053420
[21] Kalugin N G and Rostovtsev Y V 2006 *Opt. Lett.* **31** 969
[22] Wang H H, Wang L, Wei X G, Li Y J, Du D M, Kang Z H, Jiang Y and Gao J Y 2008 *Appl. Phys. Lett.* **92** 041107
[23] Shore B W, Bergmann K and Oreg J 1992 *Z. Phys. D* **23** 33
[24] Longhi S 2005 *J. Opt. B* **7** L9
[25] Dreisow F, Szameit A, Heinrich M, Nolte S, Tunnermann A, Ornigotti M and Longhi S 2009 *Phys. Rev. A* **79** 055802
[26] Imeshev G, Arbore M A, Fejer M M, Galvanauskas A, Fermann M and Harter D 2000 *J. Opt. Soc. Am. B* **17** 304
[27] Hum D S and Fejer M M 2007 *C. R. Phys.* **8** 180
[28] Suchowski H, Prabhudesai V, Oron D, Arie A and Silberberg Y 2009 *Opt. Express* **17** 12731
[29] Suchowski H, Oron D, Arie A and Silberberg Y 2008 *Phys. Rev. A* **78** 063821
[30] Bloch F 1946 *Phys. Rev.* **70** 460
[31] Feynman R P, Vernon E L and Hellwarth R W 1957 *J. Appl. Phys.* **28** 49